Geochemistry Geophysics Geosystems G3

Article
Volume 11, Number 5
21 May 2010
Q05005, doi:10.1029/2009GC002863
ISSN: 1525-2027

Published by AGU and the Geochemical Society

Equatorial paleomagnetic time-averaged field results from 0–5 Ma lavas from Kenya and the latitudinal variation of angular dispersion

Neil D. Opdyke
Department of Geological Sciences, University of Florida, Gainesville, Florida 32611, USA (drno@ufl.edu)

Dennis V. Kent
Department of Earth and Planetary Sciences, Rutgers, State University of New Jersey, Piscataway, New Jersey 08854, USA

Also at Lamont-Doherty Earth Observatory, Earth Institute at Columbia University, Palisades, New York 10964, USA

Kainian Huang and David A. Foster
Department of Geological Sciences, University of Florida, Gainesville, Florida 32611, USA

J. P. Patel
Department of Physics, University of Nairobi, PO Box 30197-00100, Nairobi, Kenya

[1] Lavas of Pliocene-Pleistocene age were sampled in two regions in Kenya: Mount Kenya on the equator and the Loiyangalani region, east of Lake Turkana, at about 3°N. We sampled 100 sites distributed around the Mount Kenya Massif and to the northeast along the Nyambini Range. The equator bisects Mount Kenya, and all sites were sampled within 40′ of the equator. Thirty-two sites were sampled in the Loiyangalani area, making a total of 132 sites. Many sites from the Mount Kenya study were severely affected by lightning; however, after progressive AF demagnetization 69 sites yielded directions with α_{95} equal to or less than 10°. Normal polarity sites dominate (N = 58 and a mean of declination (dec) = 1.2°, inclination (inc) = −0.7°, and α_{95} = 3.6°) with only 11 reverse polarity sites (mean of dec = 182.3°, inc = 0.6°, and α_{95} = 7.2°); no transitional directions were identified. Inverting the reverse sites yields a combined mean direction of dec = 1.4°, inc = −0.7°, and α_{95} = 3.2°. This result is not significantly different from what is expected from the geocentric axial dipole for the mean locality (dec = 0° and inc = 0°); a quadrupole component was not resolved. The samples from the Loiyangalani region were not seriously affected by lightning, and all 32 sites gave satisfactory data with α_{95} less than 10° (17 reverse sites, dec = 183.4°, inc = 0.8°, and α_{95} = 6.7°; 15 normal sites, dec = 358.6°, inc = −1.1°, and α_{95} = 4.7°); after inverting the reverse sites the combined mean was dec = 1.1°, inc = −1.0°, and α_{95} = 4.1°. Altogether, we had a total of 101 successful sites. A virtual geomagnetic pole (VGP) was calculated from each site mean; the VGP dispersion is low, with Sb = 10.9° for Mount Kenya and 9.8° for the Loiyangalani region. This dispersion agrees with updated Model G of McElhinny and McFadden (1997) and model TK03 of Tauxe and Kent (2004) that was tuned to the compilation of McElhinny and McFadden (1997) but disagrees with the higher dispersion near the equator and the smaller latitudinal gradient in dispersion estimated by Johnson et al. (2008). A new database is presented, and the included studies support a systematic decrease of dispersion from high to low latitudes.

Components: 10,629 words, 12 figures, 3 tables.

Keywords: paleosecular variation; Kenya; Pleistocene; paleomagnetism; Pliocene.

Index Terms: 1522 Geomagnetism and Paleomagnetism: Paleomagnetic secular variation.

Received 18 September 2009; **Revised** 21 December 2009; **Accepted** 13 January 2010; **Published** 21 May 2010.

Opdyke, N. D., D. V. Kent, K. Huang, D. A. Foster, and J. P. Patel (2010), Equatorial paleomagnetic time-averaged field results from 0–5 Ma lavas from Kenya and the latitudinal variation of angular dispersion, *Geochem. Geophys. Geosyst.*, *11*, Q05005, doi:10.1029/2009GC002863.

1. Introduction

[2] The study reported here is a follow up to work reported on equatorial lavas from Ecuador, which suggested a contribution from a quadrupole of about 5% to the time-averaged field [*Opdyke et al.*, 2006]. The present study is designed to see if this result can be replicated at another equatorial site. Therefore field collecting began in August 2006 in the Loiyangalani and Mount Kenya regions of Kenya (Figure 1). An early paleomagnetic survey of Neogene lavas in Kenya was carried out by *Reilly et al.* [1976] but their results were insufficient to test for a small quadrupole component.

2. Geology

[3] This study utilized the Pliocene to Recent volcanic flows in Kenya. The geology of Kenya is dominated by the Gregory Rift Valley which effectively bisects the country, extending from Lake Turkana in the north to Tanzania in the south, between 36°E and 37°E longitude. The Rift formed in the Precambrian shield of East Africa. The Rift Valley proper is heavily faulted and these normal faults are aligned along the axis of the rift in a NNE to SSW direction. The extension from the Miocene to the present has enabled magma to erupt along fissures or volcanoes. A series of volcanoes are present in the Rift Valley from 2.63°N at South Island in Lake Turkana to Suswa at 1.175°S; between these end points there are no less than 12 volcanoes situated about every 0.3° of latitude, mostly Pleistocene to Recent in age, some with historical flows.

[4] East of the Rift Valley and virtually on the equator is the huge volcanic edifice of Mount Kenya (Figure 2), which dates to 3 Ma and younger [*Baker et al.*, 1971]. The detailed geology of Mount Kenya is described by *Baker* [1967]. To the northeast of Mount Kenya is the Nyambeni Hills [*Rix*, 1967], which are an extension of the Mount Kenya volcanic field and range in age from 0.46 to 4.5 Ma [*Brotzu et al.*, 1984]. The volcanicity of Mount Kenya and the Nyambeni Hills seems to be synchronous. These volcanic centers are out of the Rift Valley and consequently are unaffected by the extensional tectonics associated with rifting. The lavas from Mount Kenya are dominantly basalts, rhomb porphyries, phonolites, kenytes and trachytes [*Baker*, 1967] and therefore make good magnetic recorders.

[5] In the north of Kenya, east of Lake Turkana, are two eruptive centers: Mount Kulal, east of Loiyangalani, and Longipi to the southeast (Figure 3). Mount Kulal at about 2.65°N seems to be mostly composed of Matuyama age lavas [*Gathogo et al.,* 2008]. Farther to the northeast is the Pliocene to Quaternary Hurri Hills at about 3.5°N latitude, with ages ranging from 1.4 to 2.3 Ma [*Brotzu et al.*, 1984; *Class et al.*, 1994]. Mount Marsabit at 2.25°N yields an age of about 0.6 Ma [*Brotzu et al.*, 1984]. The Barrier volcanic complex forms the volcanic edifice at the south end of Lake Turkana and is composed of four overlapping shield volcanoes: Kakorinya, east and west Likalu, and Kalolenyang. The last eruption in the region was in 1921. To the southwest of Mount Kulal is the Longipi eruptive center that is dominated by basaltic lavas. The geology of the area has been studied by the Kenya Geological Survey [*Ochieng et al.*, 1988] and in the area of interest more recently by *Gathogo et al.* [2008] who have correlated the sedimentary formations and lavas of the region to rocks of the same age in the Omo–Turkana Basin. The authors name, describe and date new basalt units that are present in the stratigraphic sequence (Figure 4); these are the Kankam Basalt (3.2 and 3.3 Ma), the Lenderet Basalt (2.02 to 2.18 Ma) and Balo Basalt (1.79 Ma). These authors also give dates for lavas from Mount Kulal (2.04 and 2.40 Ma) and Sasima Gorge (0.77 Ma). Paleomagnetic sites have been drilled from all these units except the Balo Lavas.

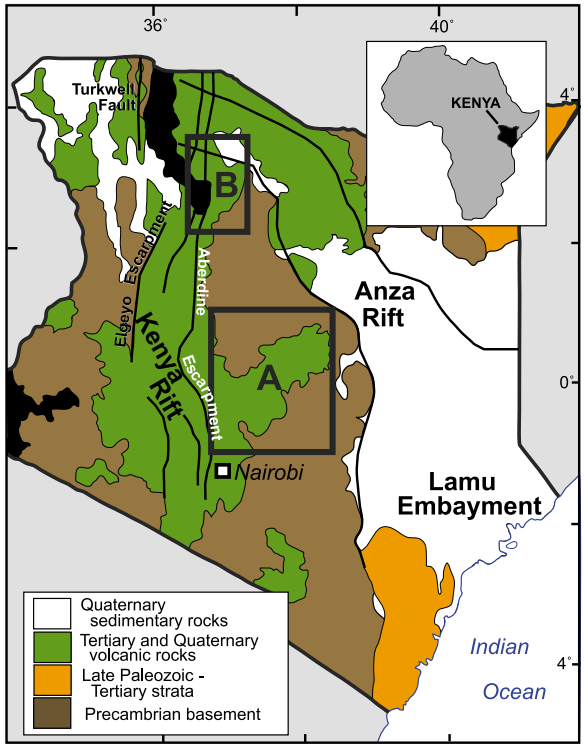

Figure 1. Geological map of Kenya modified from *Foster and Gleadow* [1996]. The boxes show the locations of the detailed maps in Figure 2 (box A) and Figure 3 (box B).

One site (KFU) was mistakenly drilled in a Miocene lava and was not used in the final statistics.

[6] The Mount Kenya region can be reached by a paved highway (A2 and B6) in good condition that circles the mountain at lower elevations, giving access to all sides of Mount Kenya. Mount Kenya is usually cloud covered and the upper reaches of the mountain are covered by forest. The summit is in the Alpine zone accessible only by foot. Lateral roads sometime allow access to higher elevations on the mountain. A road (C91) also trends northeast from the town of Meru leading to Meru National Park passing through the Nyambini Hills. All of these roads provide roadside exposures as well as lateral tracks where the roadbed itself exposes rock outcrops. The mountain is also the source of many rivers that provide good fresh outcrops where crossed by the highways.

[7] The Loyangalani area is difficult to access and only one road (C77) approaches from the south and proceeds north to a village called Gus where a road north to Koobi Fora leaves C77; another local track east of Emolo village trends to the north and gives access to lavas of Pliocene-Pleistocene age. Sampling sites are available in dry streambeds, roadside exposures and roadbeds. The sites were usually separated by hundreds of meters and were also at different elevations to try to avoid sampling the same lava multiple times. Generally this worked well but in at least one case we believe that two sites sampled the same flow since the directions are almost identical. The results from these two sites have been combined. Our intention was to return in 2008 and sample the Mount Kulal region more extensively. Unrest in Kenya prevented us from carrying out this plan. However, 32 sites were sampled in the area in 2006 and these are reported here.

[8] Sampling was carried out by drilling cores 2.5 cm in diameter of varying length, usually less than 10 cm, using a handheld gasoline-powered engine with a water swivel. The samples were oriented using a Brunton magnetic compass and a sun compass where possible. Ten samples were taken at each site usually spread over several meters of outcrop to minimize the chance that all samples at a site would be affected by the same randomizing effect, such as a single lightning strike or as part of a large rolled boulder. We sought outcrops that were as unaltered as possible. 100 sites were sampled in the Mount Kenya region (Figure 2) and 32 in the Loiyangalani (Figure 3) for a total of 1320 independently oriented core samples.

3. The $^{40}Ar/^{39}Ar$ Data

[9] Samples of the selected lavas were analyzed in the $^{40}Ar/^{39}Ar$ laboratory at the University of Florida [*Foster et al.*, 2009]. Fresh groundmass concentrates of the lavas weighing 50–200 mg were wrapped in Al foil and loaded into a quartz glass tube along with 1 mg packages of the flux monitor GA1550 biotite. Flux monitor packages were placed between every two basalt samples in the quartz tubes. The samples and flux monitors were then irradiated at the Oregon State reactor facility for 6 h. Samples were degassed using a double vacuum resistance furnace attached to a stainless steel extraction and clean-up line. Reactive gasses were removed with SAES getters prior to expansion to the mass spectrometer. Argon isotopes were analyzed using a MAP215–50 mass spectrometer with a Balzers electron multiplier. The data were reduced using ArArCALC [*Koppers,* 2002], and apparent ages were calculated using an age of 98.79 ± 0.96 Ma for GA1550 biotite standard [*Renne et al.*, 1998].

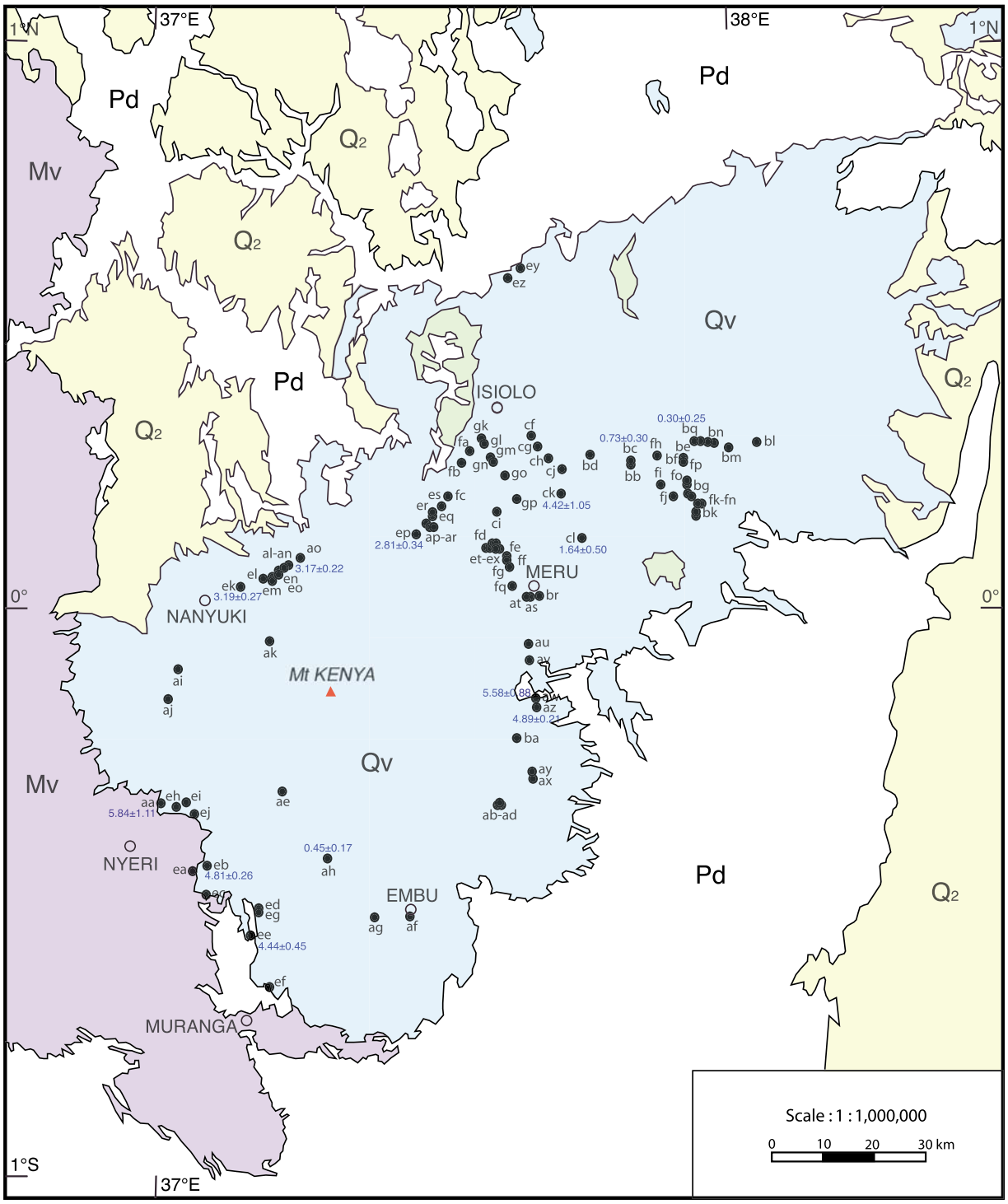

Figure 2. Site locations of Mount Kenya region on 1/1,000,000 geological map of Kenya. Radiometric dates are shown placed beside sites where appropriate.

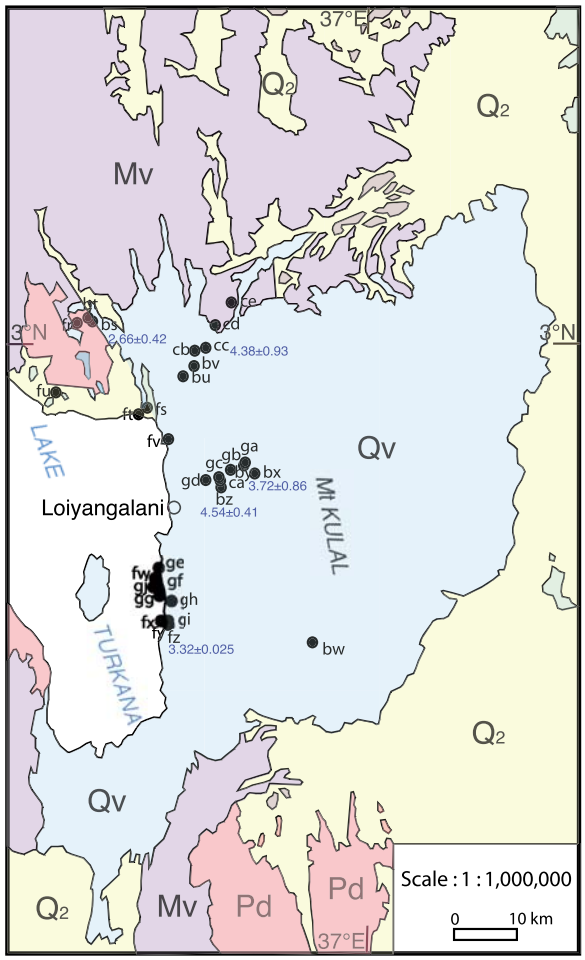

Figure 3. Site locations of Loiyangalani region on 1/1,000,000 geological map of Kenya. Radiometric dates are shown placed beside sites where appropriate.

[10] The analytical data for all of the samples is given in the auxiliary material.[1] Age spectra and inverse isochron diagrams are presented in the auxiliary material and summary of the $^{40}Ar/^{39}Ar$ age results is given in Table 1. The samples gave $^{40}Ar/^{39}Ar$ ages ranging from about 5 Ma to <0.5 Ma. Several additional samples were also analyzed but the data were highly discordant due to posteruption alteration and weathering.

[11] Sample KAA gives a highly discordant age spectrum indicative of excess argon. The inverse isochron diagram shows scatter larger than analytical uncertainty (MSWD > 4) with a $^{40}Ar/^{36}Ar$ ratio greater than atmosphere, which is also consistent with contamination with excess argon. The error isochron of 5.78 ± 1.09 Ma is the best estimate of the age of the lava at site KAA. The age spectrum from sample KAH is saddle shaped indicating contamination with excess argon in the low- and high-temperature release steps. Three steps in the middle of the spectrum give a concordant miniplateau comprising 41% of the gas with an age of 0.46 ± 0.18 Ma. Sample KAM gives a mildly discordant (MSWD = 2.32) error plateau age of 2.90 ± 0.18 Ma for 63% of the gas. The inverse isochron for the steps comprising the plateau also shows minor scatter but give a similar age and a $^{40}Ar/^{36}Ar$ ratio within error of atmosphere. The age spectrum from sample KAW is very discordant and, like sample KAA, does not reveal the age of the lava. An inverse isochron for the KAW experiment gives an age of 5.71 ± 1.00 Ma with a $^{40}Ar/^{36}Ar$ ratio greater than atmosphere. Sample KAZ gives a more concordant age spectrum then the previous samples with an error plateau age of 4.96 ± 0.19 Ma (MSWD = 3.52). The inverse isochron for KAZ show some excess scatter (MSDW = 3.44), and a $^{40}Ar/^{36}Ar$ ratio within error of atmosphere.

[12] Samples KBC and KBQ both give ages less than 1 Ma. The low-temperature release steps from KBQ show no radiogenic argon. The higher-temperature steps give a plateau age of 0.47 ± 0.17 Ma. The isochron for these steps is not very precise because of the low radiogenic argon yield, but is nevertheless within error of atmosphere. The age spectrum from KBC is more discordant. This sample, however, gives an isochron age of 0.77 ± 0.31 Ma with a $^{40}Ar/^{36}Ar$ intercept greater than atmosphere. The isochron indicates that the discordance in the age spectrum is due to excess argon and, therefore, the isochron age is considered the best estimate of the age of lava.

[13] Sample KCL gives a discordant age spectrum with a poorly defined miniplateau age of 1.72 ± 0.52 Ma. An isochron of 85% of the gas released, however, gives an age of 1. Ten ± 0.31 Ma. The greater than atmospheric $^{40}Ar/^{36}Ar$ ratio indicates that the discordance in the age spectrum is due to excess argon so that the isochron age is the preferred age of the lava.

[14] Samples KEB, KEE and KEK give ages between about 3 and 5 Ma. Sample KEB gives a discordant age spectrum with an error plateau age of 4.99 ± 0.27 Ma for 64% of the gas released. The isochron for these steps shows excess scatter and an apparent $^{40}Ar/^{36}Ar$ ratio less than atmosphere. This is probably due to some weathering or alteration of the sample and associated introduction of excess argon or argon recoil effects during irradiation. The

[1] Auxiliary material data sets are available at ftp://ftp.agu.org/apend/gc/2009gc002863. Other auxiliary materials are available in the HTML.

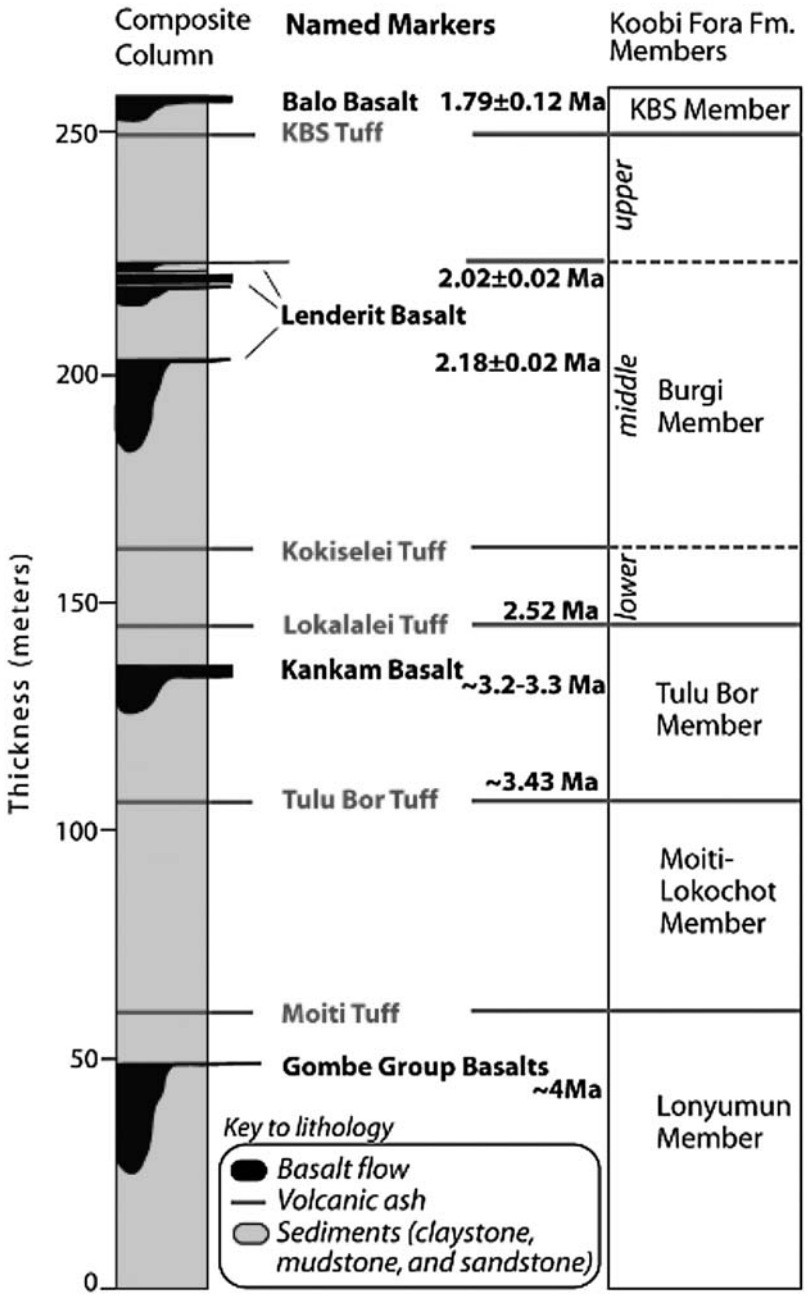

Figure 4. Lithostratigraphy of the Loiyangalani region after *Gathogo et al.* [2008].

age of this sample should be treated with caution as it may overestimate the actual age of the lava. The age spectrum from sample KEE gradually increases in age from low- to high-temperature release steps. The K/Ca ratios of the steps show the inverse and decrease at high temperatures. This suggests that the low-K phases in the sample contain some excess argon. An elevated $^{40}Ar/^{36}Ar$ ratio for the isochron also indicates the presence of excess argon. The isochron, however, is relatively well resolved and gives and age of 4.59 ± 0.44 Ma, which is considered the best age for this lava. Sample KEK gives a well-defined plateau age of 3.01 ± 0.21 Ma.

[15] The age spectra from samples KBZ, KCC, and KFZ are all discordant. Sample KBZ gives an age spectra with a minimum age of 4.84 ± 0.44 Ma based on four relatively less discordant steps. The KBZ isochron is highly scattered and the K/Ca

Table 1. Mount Kenya $^{40}Ar/^{39}Ar$ Data[a]

Site	Age (Ma)	Error (Ma)	Comments
KAA	5.78	1.09	Error isochron, $^{40}Ar/^{36}A$ r = 435 ± 33, MSWD = 4.19
KAH	0.46	0.18	Miniplateau, 41% of the gas
KAM	2.90	0.18	Error plateau age, 63% of gas
KAW	5.71	1.00	Isochron age, MSWD = 1.68, $^{40}Ar/^{36}Ar$ = 457 ± 80
KAZ	4.96	0.19	Plateau age, steps 1–12
KBC	0.77	0.31	Isochron age, MSWD = 1.29, $^{40}Ar/^{36}Ar$ = 407 ± 88
KBQ	0.47	0.17	Plateau age, 54% of gas
KCL	1.72	0.52	Miniplateau, 27% of gas
	1.10	0.31	Isochron age, 85% of gas, MSWD = 1.55, $^{40}Ar/^{36}Ar$ = 516 ± 79
KEB	4.99	0.27	Error plateau age, 64% of gas
KEE	4.59	0.44	Isochron age 100% of gas, MSWD = 1.12, $^{40}Ar/^{36}Ar$ = 839 ± 150
KEK	3.01	0.21	Plateau age, 99.7% of gas
	2.57	0.41	Isochron age = 3.34 ± 0.34, MSWD = 1.69, $^{40}Ar/^{36}Ar$ = 282 ± 53
KBS	2.45	0.39	Plateau age, 71% of gas
KBY	3.9	0.9	Miniplateau age, 25% of gas
KBZ	4.84	0.44	Error miniplateau, 47% of the gas, (maximum age)
KCC	4.51	0.96	Isochron age, MSWD = 0.49, $^{40}Ar/^{36}Ar$ = 474 ± 20
KFZ	3.64	0.28	Error miniplateau, 42% of the gas

[a]Errors are one sigma and include error in J and the decay constant.

ratios are variable suggesting gas released from several different phases. Release steps in the middle of the age spectra from KFZ give an error plateau (miniplateau) age of 3.64 ± 0.28 Ma. The K/Ca ratios of these steps gradually increase, however, suggesting that this apparent age is a mixture. The age spectrum from sample KCC gives anomalously old ages of ca. 11 Ma suggesting excess argon. The inverse isochron from KCC, however, gives an age of 4.51 ± 0.96 Ma and a MSWD of 0.49. The data from KBZ, KCC, and KFZ do not give precise ages, but were most likely erupted between 3 and 5 Ma.

4. Paleomagnetic Data

[16] The cores were returned to the United States and sliced into samples approximately one centimeter in length and measured on a 2G cryogenic magnetometer at the University of Florida. All samples were demagnetized using either thermal or alternating field demagnetization using commercial instruments. Magnetic hysteresis curves to 1 Tesla were measured on selected samples from selected sites on the Micromag (Figure 5). The resulting plot of hysteresis parameter ratios (Figure 6) showed that the samples from Kenya fell predominantly in the pseudosingle domain region [*Day et al.*, 1977], with a handful of sample Mr/Ms ratios extending into the single-domain region, all consistent with the generally fine-grained textures of the rapidly chilled basaltic lavas. The Kenya lavas were thus expected to yield stable magnetizations.

[17] The results of demagnetization were analyzed using vector end point diagrams and directions of magnetization were determined using principal component line fitting [*Kirschvink*, 1980]. Three or more points were usually employed to determine the direction. If the line did not trend toward the origin the data from the sample was not used in the analysis. Demagnetization characteristics for four sites from Mount Kenya to both thermal and AF demagnetization are illustrated in Figures 7 and 8. If the NRM directions from the samples of a site were well grouped thermal demagnetization was typically employed but if the site showed evidence of lightning affects such as high scatter or very high magetizations, then AF demagnetization was used. Most sites showed good grouping for the majority of the samples with either AF or thermal demagnetization. Site KCK (Figures 7 and 8) illustrates a site with low scatter for 8 samples from Mount Kenya with 2 samples being aberrant. The reason for the aberrant directions in this case is not clear. It can be seen in the vector end point diagram that the direction trends directly to the origin; possibilities for the deviating directions may be misorientation or displaced outcrop.

[18] Following our experience on the Mount Kenya lavas we used progressive AF demagnetization to 100 mT on all sites from the Loiyangalani area. Some sites did not entirely decay to the origin and in those cases thermal demagnetization was combined with the AF demagnetization which yielded excellent results (Figures 8a–8c) and in some cases

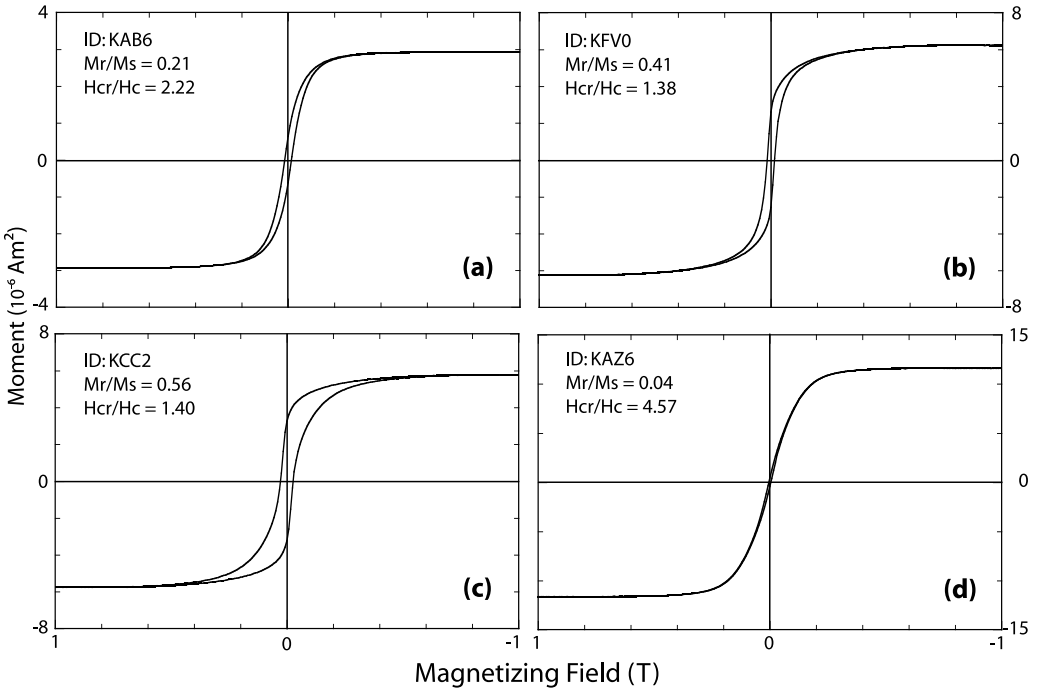

Figure 5. Magnetic hysteresis data from selected samples from Kenya. Representative hysteresis curves for samples from Mount Kenya (KAB6, KAZ6) and Loiyangalani (KFVO, KCC2). (a) KAB6, (b) KFVO, (c) KCC2, and (d) KAZ6.

resulted in very tight grouping. Three sites were believed to be individual units when sampled, but it turned out that two separate flows were sampled with different polarity at each of these sites. KGJ is one such site and shown in Figures 7 and 8 where normal and reverse polarity directions are clearly delineated. Considerable time must have elapsed between the emplacement of these two flows with opposite polarity, certainly in excess of 10,000 years.

4.1. Mount Kenya Results

[19] Site statistics were calculated using *Fisher* [1953] statistics. The acceptance of sites for fur-

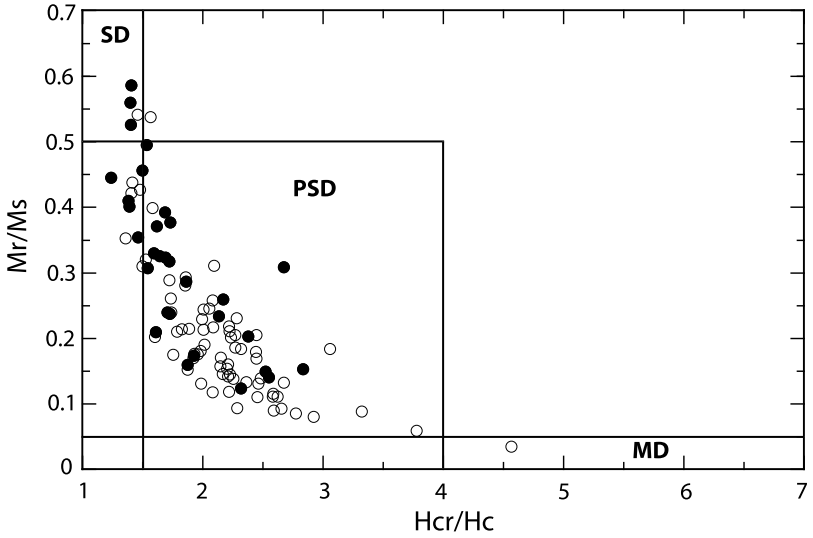

Figure 6. Plot of hysteresis parameter ratios (Mr/Ms versus Bcr/Ms) for samples from sites from Mount Kenya (open circles) and Loiyangalani (filled circles). Delineation of single-domain (SD), pseudosingle domain (PSD), and multidomain (MD) behavior from *Day et al.* [1977].

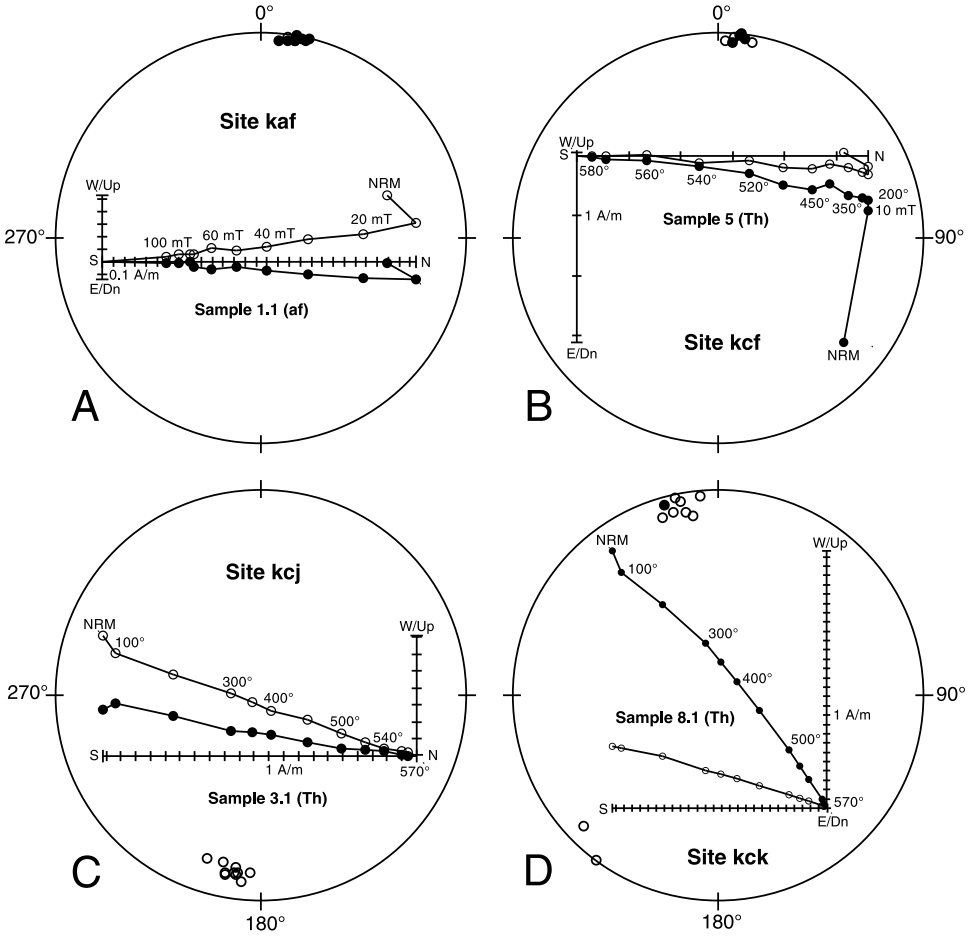

Figure 7. Vector end point diagrams of results from four Mount Kenya sites. The vector end point diagram from site KCK is from one of the aberrant samples from this site.

ther analysis rests on sites with N greater than 5 and with α_{95} less than 10°; these criteria led to the elimination of 30 sites. Most of the sites with a high α_{95} were most probably affected by lightning although one site had very low coercivity and did not yield a stable result. Of the 69 accepted sites, 11 sites had reverse polarity magnetizations while 59 had normal polarity magnetizations, but none showed intermediate directions. This is remarkable in a collection of this size, which may be the result of the small number of reverse polarity sites in the data set. The directional distribution of the normal polarity sites (declination (dec) = 1.2°, inclination (inc) = −0.7°, α_{95}° = 3.6°, N = 59) and reverse polarity sites (dec = 182.3°, inc = 0.6°, α_{95}° = 7.2°, N = 11) are shown in Figure 9a; the mean directions are clearly bipolar and pass a reversal test having overlapping α_{95}. The reverse directions were therefore inverted and an overall mean was calculated of the combined data set of N = 69 sites with a result (dec = 1.4°, inc = −0.7, α_{95} = 3.2°) that is not significantly different from the geocentric axial dipole field for the Mount Kenya area (dec = 0°, inc = 0°). The site statistics are given in Table 2.

4.2. Loiyangalani Results

[20] The results from progressive AF demagnetization were excellent and the site data are presented in Table 2. There are 31 sites which gave acceptable results using α_{95} less than 10° as the cutoff value. All site means had precision parameters, k, higher than 50 and 19 sites had k values greater than 100. It is interesting that at three of the localities both normal and reverse samples were measured. Locality KFW yielded 5 normal and 4 reverse samples, with tight grouping for the normal samples (k = 205) and somewhat less well for the reverse samples (k = 60). Site KGJ also yielded both polarities (Figure 9b) with both polarities being well grouped (with k = 303 for the n = 5 normal and k = 242 for the n = 4 reverse samples); both sites were included in the final

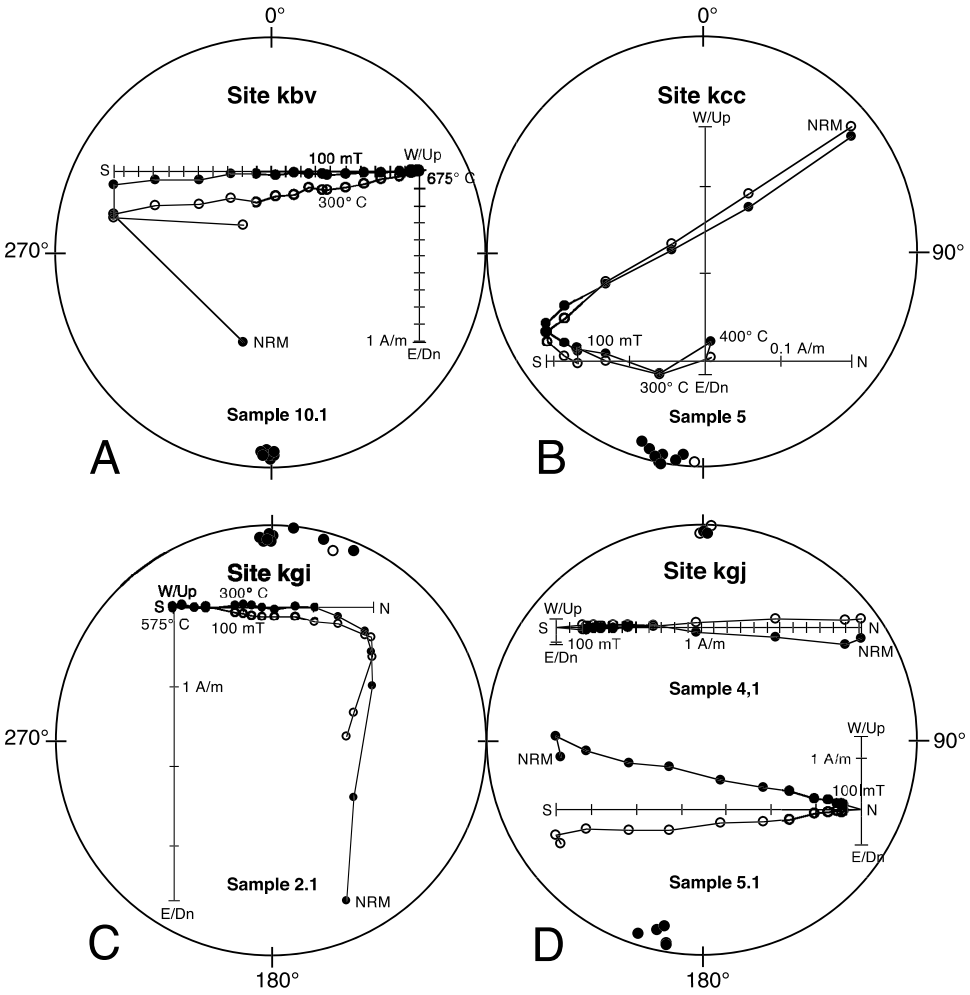

Figure 8. Vector end point diagrams of samples from four sites from the Loiyangalani region.

statistics. In the field we did not realize that two different flows were sampled; this is difficult to determine sometimes in limited roadside or road-bed exposures. It is interesting to note that none of the sites yielded intermediate directions. Hiatuses of several thousands of years evidently must have elapsed between flows and eruption rates may be lower than in some other volcanic provinces where intermediate lava directions are not uncommon (i.e., Hawaii).

[21] Only two sites had unacceptably high dispersion (KFY and KEW-R); usually more sites are rejected for high scatter and in the case of the study of Mount Kenya lavas, 30% of the sites were rejected. The very high success ratio for results from the Loiyangalani region must result from low incidence of lighting strikes to ground, perhaps because of the arid climate in the area. The results represent both normal (13) and reverse (17) site mean directions varying in age from about 4.18 to 0.77 Ma (see above). The normal sites (N = 15, dec = 358.6°, inc = −1.1°, α_{95} = 4.7°, k = 67) and the reverse sites (N = 17, dec = 183.4°, inc = 0.8°, α_{95} = 6.7°, k = 29) are antipodal and have overlapping circles of confidence. As a result the reverse data can be inverted giving a combined mean direction for N = 32 of dec = 1.1°, inc = −1.0, α_{95} = 4.1°. The inclination anomaly (ΔI) is 6° and the combined mean VGP (latitude = 86.5°N, longitude = 197.6°E, A_{95} = 2.9°) is slightly far-sided with respect to the expected geocentric axial dipole field for this latitude.

5. Dispersion of the Paleomagnetic Field

[22] The present study was initiated as a result of a study of equatorial lavas in Ecuador [*Opdyke et al.*, 2006] where we found that the data was compatible with a 5% quadrupole field contribution to a dominant dipole field. This observation led to the

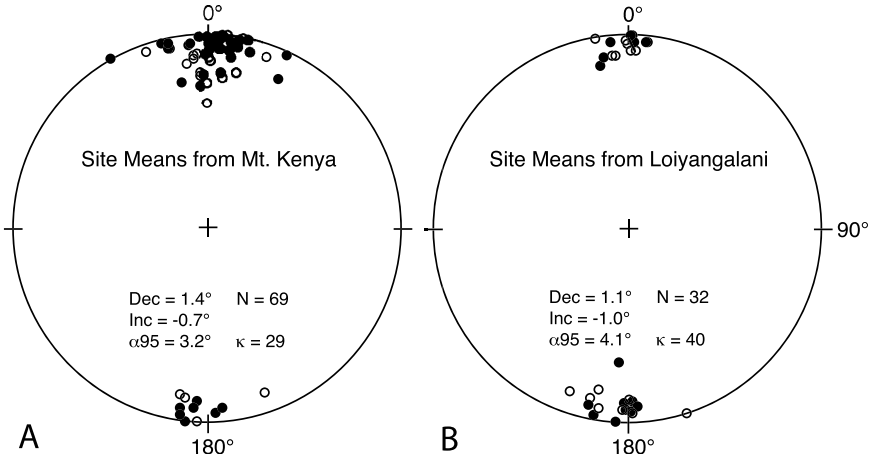

Figure 9. Site mean directions from sites from Kenya plotted on a stereographic projection. Filled circles indicate sites with mean inclinations dipping below the horizon, while open circles indicate sites with inclinations above the horizon.

hypothesis that if this were generally true then in Kenya at 3°N we should observe a field that was essentially horizontal [*Wilson*, 1970, 1972]. This is what we do in fact observe. At Mount Kenya (at the equator) we observe only the dipole field with the inclination horizontal (Figure 10). The available data at latitudes less than 15° are presented in the inset in Figure 10. Five of the six results available from latitudes less than 15° would agree with a 5% quadrupole field being present at equatorial latitudes. The exception is Mt Kenya.

[23] Figure 11 is based on an updated and expanded data set (Table 3) based on modern paleomagnetic analysis using AF or thermal demagnetization and line fitting analysis to define the characteristic component. The studies presented in Table 3 were chosen based on the criteria given above for the present study: studies were screened and sites were eliminated when the number of samples fell below 5 or the α_{95} exceeded 10°. This selection sometimes reduced the number of acceptable sites below 30 or in some cases 20; such studies are therefore classified as second tier. The number of sites in modern (e.g., Time-Averaged Field Initiative) studies have been steadily increasing so that now studies that include 50 or more sites are the norm and in some cases exceed 100. We included studies in which the data were presented as appendices by *Johnson et al.* [2008]. It is hoped that these data will soon be published since some of these studies have problems that can only be addressed by full presentation of the data. It is interesting that in certain cases such as Iceland the number of sites that meet the minimum criteria outlined above is only 35 even though thousands of measurements have been made on Icelandic lavas but usually on 4 or fewer samples per site; more samples per lava will have to be collected to increase the precision, as was done by *Udagawa et al.* [1999]. Table 3 has 28 areas in which data are presented, some of these represent combined results from two or more studies, for example, Mexico and the western United States.

[24] The data presented in Table 3 and Figure 11 are, for the most part, strongly dipolar. Most have an α_{95} that includes the present rotation axis, 5 localities have α_{95} that are within a degree of the rotation axis, but 4 are offset from the rotation axis by as much as 4° (including our results from Loiyangalani). Figure 11 shows clearly that the normal directions are strongly dipolar; however, the reverse directions from the southern hemisphere seem to have values that are consistently shallow but in the northern hemisphere there does not seem to be a bias. A polarity asymmetry in directions was also observed in equatorial deep-sea sediment cores, suggesting there is a standing (nonreversing) component of the geomagnetic core field [*Schneider and Kent*, 1988]. More data are required to resolve the significance of these observations.

[25] The latitudinal variation in dispersion variation is shown in Figure 12; the data are listed in Table 3. We have added new studies as they become available and built upon the original compilation published in 2004 [*Opdyke and Mejia*, 2004]. We have recalculated the results from the original studies using the criteria given above, the only exception being the data from Easter Island [*Brown*, 2002], which has 4 samples per site to which we have added the sites of *Miki et al.* [1998].

Table 2. Site Statistics for Kenya Lavas

Site	Site Latitude	Site Longitude	N	Dec	Inc	α_{95}	κ	P	VLat	VLon	Age
KAA	0°21.44′S	37°00.47′E	10	177.5	5.8	4.3	126	R	−86.5	81.9	
KAB	0°21.22′S	37°36.79′E	9	10.7	−0.7	6.2	69	N	79.3	127.4	
KAC	0°21.33′S	37°36.71′E	10	74.3	23.4	21.3	7				
KAD	0°21.33′S	37°36.71′E	10	4.1	−8.6	5.3	85	N	84.3	171.4	
KAE	0°40.57′S	37°13.53′E	6	13.3	8.0	9.6	49	N	75.9	107.5	
KAF	0°32.70′S	37°26.93′E	10	9.9	1.8	1.9	665	N	80.0	119.4	
KAG	0°32.86′S	37°23.33′E	10	353	−16.1	7.2	46	N	79.6	259.3	
KAH	0°26.54′S	37°18.32′E	11	355.5	−12.3	8.0	33	N	82.6	254.9	0.45 ± 0.17
KAI	0°06.38′S	37°02.33′E	8	3.5	2.6	4.5	154	N	86.2	105.2	
KAJ	0°09.60′S	37°01.25′E	10	274.8	12.2	54	2				
KAK	0°03.39′S	37°12.09′E	7	166.5	23.5	13.6	21	R			
KAL	0°03.44′N	37°12.41′E	7	59.6	53.8	17.4	13				
KAM	0°04.11′N	37°13.16′E	6	0.3	−25.9	8.4	65	N	76.3	216	3.17 ± 0.22
KAN	0°04, 87′N	37°14.06′E	9	36.3	−15.7	26.3	5	N			
KAO	0°05.54′N	37°15.36′E	8	269.8	−12.8	27.7	5				
KAP	0°09.13′N	37°28.72′E	10	281.5	−17.5	27.5	4				
KAQ-R	0°08.57′N	37°29.03′E	14	357.3	1.5	4.7	72	N	87.2	321.0	
KAS	0°01.21′N	37°39.80′E	10	5.1	9.2	30.3	4	N			
KAT	0°01.52′N	37°39.68′E	9	19.2	−7.4	4.6	126	N	70.5	138.9	
KAU	0°03.69′S	37°39.67′E	10	175.2	8.7	4.5	118	R	−83.6	85.9	
KAV	0°05.47′S	37°39.78′E	9	183.0	−1.3	5.5	89	R	−86.9	293.7	
KAW	0°09.45′S	37°40.32′E	10	184.7	−17.6	78.6	1	R			5.53 ± 0.88
KAX	0°18′00′S	37°40.01′E	10	357.8	0.3	32.4	3	N			
KAY	0°17.24′S	37°39.92′E	10	0.6	−13.4	3.1	240	N	83.5	212.4	
KAZ	0°10.35′S	37°40.52′E	10	160.8	−11.9	7.1	47	R	−69.9	146.0	4.89 ± 0.21
KBA	0°13.73′S	37°38.33′E	10	51.1	15.3	66.8	1	N			
KBB	0°15.42′N	37°50.50′E	10	358.3	13.4	24.5	5	N			
KBC	0°15.52′N	37°50.63′E	9	2.3	2.0	5.3	95	N	87.6	110.9	0.73 ± 0.30
KBD	0°16.43′N	37°46, 79′E	8	359	22.1	5.4	107	N	78.8	32.8	
KBE	0°15.92′N	37°55.93′E	10	285.5	−1.5	20.8	6				
KBF	0°15.81′N	37°56.02′E	10	2.6	6.9	2.2	494	N	85.9	77.3	
KBG	0°13.30′N	37°56.47′E	6	350.4	18.6	10.8	39	N			
KBH	0°12.27′N	37°56.59′E	9	1.1	−14.9	6.9	56	N	82.1	209.9	
KBI	0°11.97′N	37°56.80′E	8	354.4	6.0	5.8	92	N	83.7	334.6	
KBJ	0°11.18′N	37°57.59′E	7	356.7	12.1	14.7	9	N			
KBK	0°10.38′N	37°57.46′E	10	20.7	−34.2	22.3	6	N			
KBL	0°17.77′N	38°03.85′E	7	356.7	12.1	14.7	18	N			
KBM	0°17.33′N	38°00.73′E	10	344.3	−35.4	29.5	4	N			
KBN	0°17.67′N	37°59.38′E	6	359.2	11.7	4.1	267	N	84.3	29.9	
KBO	0°17.62′N	37°59.16′E	10	5.0	21.0	4.3	129	N	78.3	63.0	
KBP	0°17.62′N	37°59.16′E	9	5.1	1.3	6.3	68	N	84.9	124.0	
KBQ	0°17.62′N	37°59.16′E	10	0.3	3.3	4.3	129	N	88.6	50.5	0.3 ± 0.25
KBR	0°01.34′N	37°35.33′E	9	356.7	−11.0	4.4	136	N	83.5	248.2	
KCF	0°18.48′N	37°34.50′E	7	5.9	−0.4	3.4	311	N	84.1	132.4	
KCG	0°17.30′N	37°35.06′E	9	345.9	2.3	5.7	81	N	75.9	311.1	
KCH	0°16.02′N	37°35.77′E	9	0.4	5.7	4.2	148	N	87.4	46.5	
KCI	0°10.36′N	37°30.88′E	7	4.5	−0.9	8.3	54	N	85.5	135.7	
KCJ	0°14.87′N	37°36.72′E	10	189.5	−14.4	2.8	305	R	−78.2	270.5	
KCK	0°12.44′N	37°37.71′E	8	348.3	−6.4	5.3	124	N	77.8	291.2	4.42 ± 1.05
KCL	0°07.56′N	37°39.76′E	9	357.4	−21.1	4.8	114	N	78.7	230.8	1.64 ± 0.50
KEA	0°27.90′S	37°03.85′E	6	186.5	0.2	8.6	61	R	−83.5	303.6	
KEB	0°27.44′S	37°05.54′E	10	357.2	27.9	3.5	195	N	74.4	27.0	4.81 ± 0.26
KED	0°31.82′S	37°11.01′E	3	4.5	−1.0	12.6	97	N			
KEE	0 °34.61′S	37°10.14′E	6	10.4	−19.9	8.1	69	N	75.8	170.6	4.44 ± 0.43
KEF	0°40.19′S	37°12.13′E	9	7.2	9.2	5.2	101	N	81.0	90.6	2.58 ± 0.73
KEG	0°31.82′S	37°11.01′E	9	25.4	16.1	7.6	46	N	63.2	107.7	
KEH	0°20.94′S	37°02.22′E	7	1.6	4.5	4.7	166	N	87.0	69.1	
KEI	0°20.50′S	37°03.15′E	8	4.0	8.3	4.1	181	N	84.0	78.8	
KEJ	0°21.71′S	37°04.08′E	9	330.5	0.2	9.4	31	N	60.5	307.8	
KEK	0°02.34′N	37°08.51′E	10	183.5	12.0	2.5	374	R	−83.0	7.2	3.19 ± 0.27
KEM	0°03.34′N	37°12.41′E	10	188.3	7.3	1.5	104	R	−80.9	331.7	
KEN	0°04.44′N	37°13.58′E	4	101.0	0.3	38.4	1				

Table 2. (continued)

Site	Site Latitude	Site Longitude	N	Dec	Inc	α_{95}	κ	P	VLat	VLon	Age
KEO	0°03.85′N	37°12.98′E	10	184.4	8.7	1.9	640	R	−83.7	352.8	
KEP	0°07.97′N	37°27.69′E	10	3.7	3.6	3.7	168	N	85.9	102.8	2.81 ± 0.34
KEQ	0°10.00′N	37°29.47′E	9	12.4	1.7	7.3	50	N	77.6	124.5	
KER	0°10.24′N	37°29.74′E	10	329.6	−13.3	35.6	3	N			
KES	0°11.04′N	37°30.42′E	10	0.1	−1.7	4.6	111	N	88.9	212.1	
KET	0°06.57′N	37°35.06′E	10	324.9	34.4	60.8	2	N			
KEU	0°06.59′N	37°35.20′E	8	9.4	6.2	5.6	99	N	80.1	109.7	
KEV	0°06.57′N	37°35.74′E	8	7.2	4.1	5.3	109	N	82.5	112.4	
KEW	0°06.51′N	37°35.97′E	10	3.2	2.2	3.7	175	N	86.6	110.2	
KEX	0°06.38′N	37°36.53′E	10	359.9	1.5	4.7	107	N	89.3	28.9	
KEZ	0°35.19′N	37°37.35′E	8	188.4	4.0	8.0	49	R	−81.2	324.8	
KFA	0°16.88′N	37°33.41′E	10	340.9	45	85	1	N			
KFB	0°15.49′N	37°32.52′E	9	358.4	6.1	16.9	10	N			
KFC	0°12.06′N	37°31.08′E	9	24.5	2.8	5.7	84	N	65.5	124.6	
KFD	0°06.52′N	37°36.13′E	10	4.3	1.6	2.3	433	N	85.6	118.3	
KFE	0°05.65′N	37°37.16′E	8	341.1	−5.1	8.4	44	N	70.9	299.5	
KFF	0°05.24′N	37°37.23′E	10	355.3	−13.8	5.7	72	N	81.5	250.9	
KFG	0°04.46′N	37°37.59′E	10	357.6	−22.9	3.6	181	N	77.7	228.7	
KFH	0°16.48′N	37°53.27′E	10	350.1	24.7	5.0	93	N	74.0	0.5	
KFI	0°13.21′N	37°56.48′E	8	7.7	12.3	6.9	66	N	80.2	89.7	
KFJ	0°11.99′N	37°57.17′E	10	354.5	5.5	5.0	94	N	83.9	333.0	
KFK	0°11.16′N	37°57.74′E	9	2.0	−6.7	7.2	52	N	85.9	188.7	
KFL	0°10.03′N	37°57.39′E	10	6.0	−23.0	4.3	128	N	76.4	192.1	
KFM	0°10.25′N	37°57.48′E	5	28.6	−27.8	45.5		N			
KFN	0°11.01′N	37°57.42′E	10	359.8	−35.6	5.9	68	N	70.1	218.6	
KFO	0°13.60′N	37°56.47′E	10	0.3	9.3	5.1	92	N	85.5	41.7	
KFP	0°15.67′N	37°56.26′E	6	4.0	−2.9	3.2	447	N	85.6	151.5	
KFQ	0°02.38′N	37°37.90′E	3	182.8	45.3	40.7	10	R			
KGK	0°18.20′N	37°34.67′E	3	15.9	3.9	11.8	110	N			
KGL	0°17.59′N	37°34.89′E	9	347.8	6.8	3.9	174	N	77.4	322.1	
KGM	0°16.32′N	37°35.58′E	11	24.7	−3.2	16.9	8	N			
KGN	0°15.71′N	37°35.92′E	6	348.0	3.1	5.1	177	N	77.9	313.6	
KGO	0°14.23′N	37°37.01′E	10	187.5	−13	4.8	103	R	−80.2	267.0	5.36 ± 1.06
KGP	0°11.66′N	37°38.35′E	8	2.1	3.6	2.0	759	N	87.4	90.3	
All			69	1.4	−0.7	3.2	29		88.5	143.3	
Normal			58	1.2	−0.7	3.6	27	N	88.7	146.6	
Reverse			11	182.3	0.6	7.2	40.9	R			
				Loiyangalani Sites							
KBS	3°01.86′N	36°36.02′E	10	199.2	−12.2	4.5	114	R	−70.6	296.5	
KBT	3°02.25′N	36°35.95′E	10	190.4	−17.2	2.9	282	R	−78.1	276.9	
KBU	2°57.14′N	36°44.07′E	10	178.5	12.7	2.3	459	R	−80.5	45.7	
KBV	2°58.10′N	36°45.10′E	11	180.7	7.6	0.9	2360	R	−83.1	30.9	
KBW	2°33.92′N	36°55.25′E	11	183.4	1.0	1.2	1439	R	−85.4	349.2	
KBX	2°48.73′N	36°50.29′E	10	1.4	0.7	5.2	86	N	87.2	187.0	
KBY	2°49.42′N	36°49.36′E	5	6.4	−4.5	6.1	161	N	81.8	165.0	3.90 ± 0.9
KBZ	2°48.67′N	36°47.39′E	9	0.2	−5.8	4.4	138	N	84.5	214.7	4.84 ± 0.44
KCA	2°48.02′N	36°47.19′E	9	176.5	9.1	3.7	198	R	−81.8	62.2	
KCB	2°58.80′N	36°45.40′E	10	181.2	11.0	4.3	129	R	−81.4	28.8	
KCC	2°59.62′N	36°45.96′E	9	190.3	3.4	3.9	177	R	−78.7	331.2	4.51 ± 0.96
KCD	3°01.63′N	36°46.91′E	10	192.6	−12.0	2.0	603	R	−77.1	292.6	
KCE	3°03.68′N	36°48.15′E	10	179.1	6.8	2.5	381	R	−83.4	44.7	
KFS	2°54.37′N	36°40.43′E	9	162.0	−0.7	2.7	354	R	−71.8	119.0	
KFT	2°53.84′N	36°40.10′E	9	183.6	32.0	3.5	221	R	−69.4	26.9	
KFU	2°55.73′N	36°33.05′E	9	355.1	−12.3	7.0	54	N	79.6	244.8	
KFV	2°51.71′N	36°42.87′E	9	178.2	−6.1	2.6	402	R	−88.2	131.7	
KFW-N	2°39.34′N	36°41.46′E	5	350.2	−1.7	5.4	205	N	79.6	286.9	
KFW-R	2°39.34′N	36°41.46′E	4	181.3	32.2	11.9	60	R			
KFX	2°35.80′N	36°42.12′E	10	2.5	−9.6	5.4	271	N	82.2	198.1	
KFY	2°35.76′N	36°42.31′E	10	359.7	−4.2	6.4	59	N	85.3	220.4	
KFZ	2°35.30′N	36°42.59′E	9	350.7	16.2	4.0	170	N	79.1	338.5	3.64 ± 0.28
KGA	2°49.60′N	36°49.62′E	10	1.9	4.5	4.2	131	N	88.0	142.8	

Table 2. (continued)

Site	Site Latitude	Site Longitude	N	Dec	Inc	α_{95}	κ	P	VLat	VLon	Age
KGB	2°49.01′N	36°48.24′E	10	1.3	−9.9	5.2	89	N	82.1	207.3	
.KGC	2°48.15′N	36°47.26′E	10	354.6	4.1	4.9	96	N	84.6	299.0	
KGD	2°48.03′N	36°46.08′E	10	189.2	−7.5	2.7	315	R	−80.8	300.5	
KGE	2°40.33′N	36°41.86′E	10	181.5	−7.4	2.3	449	R	−88.2	272.5	
KGF	2°38.61′N	36°41.86′E	8	355.9	−11.9	6.4	77	N	80.5	242.1	
KGG	2°37.96′N	36°41.93′E	7	179.3	−13.6	8.0	58	R	−85.6	207.5	
KGH	2°37.29′N	36°41.96′E	10	352.2	12.2	4.5	118	N	81.4	331.6	
KGI	2°35.77′N	36°42.39′E	10	5.5	4.5	6.5	57	N	84.5	130.2	
KGJ-N	2°38.62′N	36°41.76′E	4	1.1	0.5	5.3	303	N	87.4	191.6	
KGJ-R	2°38.62′N	36°41.76′E	5	192.6	7.8	4.9	242	R	75.8	334.0	
All			32	1.1	−1.0	4.1	39.60				
Normal			15	358.6	−1.1	4.7	66.74				
Reverse			17	183.4	0.8	6.7	29.33				
VGPs			32	197.6	86.5	2.9	77.14				

Many of these new data sets were generated by the TAFI program [*Johnson et al.*, 2008]. The data presented in Table 3 have been recalculated assuming that VGPs falling between 45°N and S are transitional and can be excluded. The dispersion Sb has been recalculated in a uniform way relative to the VGP mean pole of the data set instead of around the present axis of rotation. We present Sb with errors calculated after *Cox* [1969] and *Tauxe* [2009] using the bootstrap method. It is always tempting to increase the number of sites as much as possible, which usually means adding data with more relaxed acceptance criteria such as was done by *Lawrence et al.* [2009] in their study of results from 20° north and south of the equator.

[26] An important objective of time-averaged field studies is to determine the dispersion of the magnetic field through time and space. Usually rocks younger than 5 Ma (Pliocene and Pleistocene) are studied on the assumption that plate tectonic motion and true polar wander are negligible over this time frame. This really depends on the direction and velocity of plate motion. If it is on a fast moving plate traveling in a north–south direction like the motion of the Pacific or Indian plates, then the mean age for the data must be determined and a correction applied for this motion [*Schneider and Kent*, 1988; *Yamamoto et al.*, 2002; *Opdyke and Musgrave*, 2004]. Fortunately the African plate is moving slowly and opening of the African rift is east–west so that problems associated with plate tectonics are minimized with the Kenya data. The scatter of the data is assumed to be due to motion of the magnetic pole around the axis of rotation due to

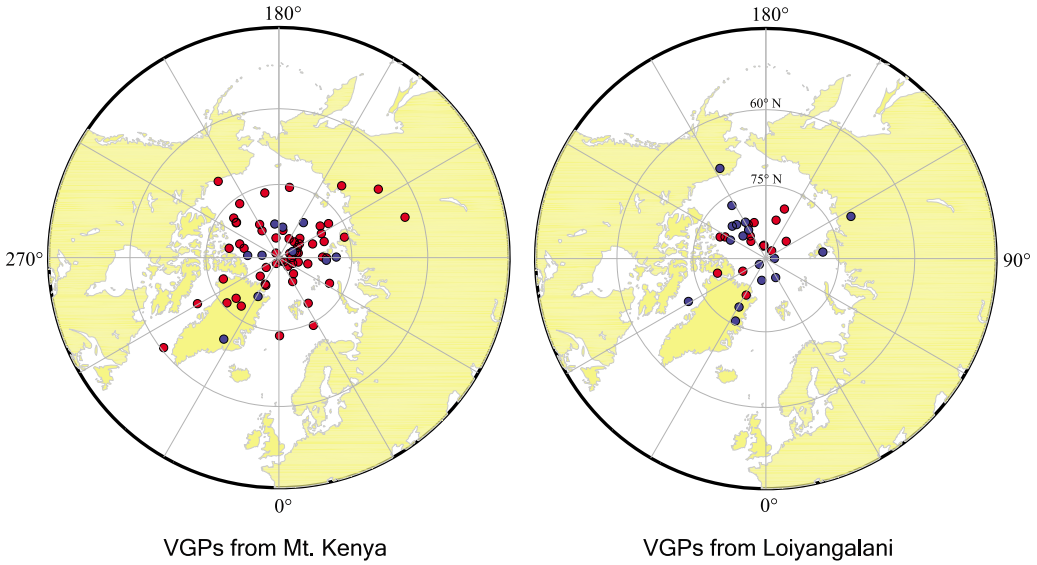

Figure 10. Virtual geomagnetic pole positions for both areas of Kenya with cutoff value of α_{95} at 10°.

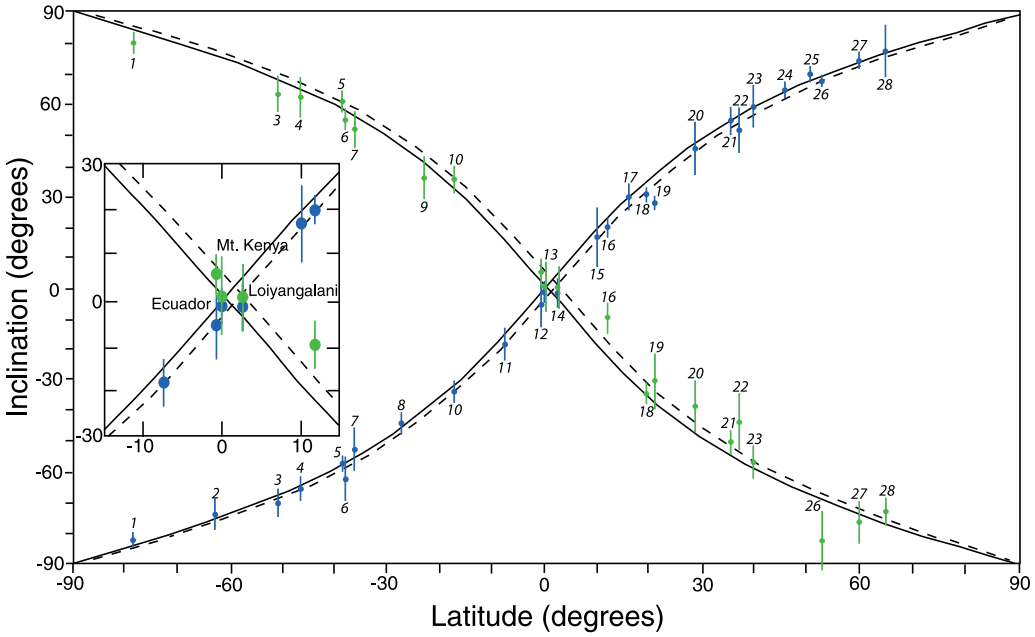

Figure 11. Mean inclination in degrees plotted against latitude for selected studies (Table 3). The expected inclination of the geocentric axial dipole is given by the solid line, and the dashed line is the expected inclination if a 5% quadrupole field is present in the data. Inset shows a blowup of the region between 15°N and 15°S latitude.

secular variation or dipole wobble. It may also be due to undetected local tectonism. The scatter of the data is usually studied by calculating a virtual geomagnetic pole (VGP) for each site [*Fisher*, 1953]. The scatter is then assessed by using a modified angular standard deviation (Sb) that takes into account dispersion within each site (Sw) and using this value to measure the scatter around the present geographic (rotation) axis [*Cox*, 1969]. This method assumes that Earth's field is predominantly axial dipolar; however; this is one hypothesis that we are trying to test in these studies. The total dispersion of the VGPs around the paleomagnetic pole is determined where each pole is an angular distance (δ I) away from the mean paleomagnetic pole. The formula we use for total angular dispersion Sb is from *Johnson et al.* [2008].

[27] We believe that the dispersion should be calculated around the mean paleomagnetic pole as calculated by *Smirnov and Tarduno* [2004] and *Biggin et al.* [2008] rather than the present axis of rotation as has been done by *Cox* [1969]. As a practical matter it makes little or no difference in a study such as this when the mean direction is virtually coincident with the geocentric axial dipole. However, it becomes important when paleodispersion is being studied in more remote times like the Precambrian when the axis of rotation can only be determined from the paleomagnetic pole.

[28] A question arises of the best way of excluding sites with subpar data. We have chosen an α_{95} of 10° but other cutoff values are often used; for example, *Johnson et al.* [2008] prefer that the concentration or precision parameter, K [*Fisher*, 1953] should be greater than 50. The analysis of our Mount Kenya data using the results of the VGPs with α_{95} less than 10° give Sb = 10.9° (95% confidence interval from 9.1° to 12.9°). However, if K > 50 or > 100 are used as the cutoff values for the Mount Kenya data set then the Sb values of the VGPs are 9.1°and 8.5°, respectively; in other words the between-site dispersion decreases as N goes from 50 to 38. What value best represents the scatter for the sampling region? This is unclear but we use the greater scatter represented by an α_{95} cutoff of 10° as we believe this to be conservative. It is interesting that this dispersion is less than observed in Ecuador but about what *Cox* [1971] observed in data from the Galapagos, which he obtained without using demagnetization of any kind. Our value (10.9°) from Mount Kenya is lower than dispersion at the equator in the original Model G [*McFadden et al.*, 1988] but agrees well with updated Model G of *McElhinny and McFadden* [1997] who estimated a dispersion of 11.1° for selected lava sites from a band within 5° of the

Table 3. Database for Dispersion With Latitude[a]

Location	Latitude (deg)	Longitude (deg)	P	N	Dec	Inc	α_{95}	Pal.Pole Latitude	Pal.Pole Longitude	A_{95}	R	K	Sb1 "T"	Sb2 "C"	References[b]
McMurdo	−78	166	C	111	13.8	−81.1	2.2	84.7	207.5	5.1	102	12	$23.7^{25}_{21.6}$	$23^{25.4}_{21.0}$	1
			N	68	12.8	−82.4	2.8	86.9	224.5	4					
			R	43	194.8	78.9	3.6	−80.8	18.4	6.5					
Deception Island	−63	299	N	13	350.4	−73.7	5.4	85.4	237.8	8.5	12.5	24.7	$16.5^{23.7}_{8.4}$	$16.3^{22.0}_{12.9}$	2
Patagonia	−51	290	C	41	1.7	−67.8	3.6	88.8	72.5	5.3	38.8	18.5	$18.8^{21.6}_{15.8}$	$18.8^{22.2}_{16.3}$	3
			N	28	2	−69.8	4.5	85.1	99.2	6.8					
			R	13	181.2	63.5	5.8	84.7	297.3	8.4					
Possession Island	−46	51.8	C	36	2	−64	3.7	88.7	165.2	5.4	34.3	20.4	$17.8^{21.8}_{13.5}$	$17.9^{21.3}_{15.4}$	4
			N	18	356.3	−65.4	3.9	86.7	277.5	5.5					
			R	18	187.2	62.5	6.5	−85	305.7	9.5					
New Zealand	−38.5	176	C	105	7.4	−58.4	2.1	84.1	284.9	2.7	101	27		$15.5^{17.2}_{14.2}$	5
			N	81	9	−57.4	2.5	82.9	273.9	3.2					
			R	24	181	61.3	3.8	−84.9	166.3	4.4					
Victoria, Australia	−38	14.5	C	36	355	−57.9	6.7	86.2	26.6	4.7	34.7	26.6	$16.2^{21.1}_{11.7}$	$15.7^{18.7}_{13.5}$	6
			N	15	356.6	−62.2	7	83.3	336.4	9.6					
			R	21	174.1	54.9	3.7	85.3	70.9	4.5					
Northern Patagonia	−36	291	C	31	357.3	−52.8	4.6	87.9	214	4.7	30	38.7	$14.6^{17.8}_{11.2}$	$13^{15.7}_{11.1}$	7
			N	19	354.8	−53	6.7	85.8	215	6.7					
			R	12	181	52.3	6	−88.8	218.9	6					
Easter Island	−27.1	250.8	N	64	357.5	−44.8	4	87.5	164.1	2.7	62.5	43.1	$12.5^{15.1}_{9.6}$	12.3^{14}_{11}	8
Atacama	−23	292	C	29	356.9	−36.2	6.6	86.2	230.6	6.4	27.5	18.5	$19.3^{22.8}_{15.6}$	$18.8^{22.9}_{16}$	9
			N	8	345	−43.8	13.4	75.4	186.8	14.5					
			R	21	180.6	33	7.3	−86	122.7	6.6					
Society Island	−17	209	C	116	1.2	−35	2.8	87.7	19.5	2.5	112	28.9		$15.1^{16.6}_{13.8}$	10
			N	73	2.5	−34.4	3.6	87.7	349.1	3.1					
			R	43	179.1	36.1	4.7	86.5	54.4	4.2					
Java, Indonesia	−7.4	112	N	35	359.6	−18.5	5.2	87.5	296.3	3.9	34.1	39.3	$13.1^{15.2}_{11.0}$	$12.9^{15.4}_{11.1}$	11
Ecuador	−0.6	282	C	51	359.9	−5.4	4.2	87.7	106	3.5	50	33.5	$14.2^{16.3}_{12.0}$	$14.0^{16.2}_{12.3}$	12
			N	21	354.6	−5	7.2	84.2	170	5.5					
			R	30	183.5	−5.6	4	−85.8	226.5	4.3					
Mount Kenya	0	36.5	C	69	1.4	−0.7	3.2	88.5	143.3	2.3	67.7	29	$11.0^{12.4}_{9.8}$	$11.0^{12.7}_{9.2}$	13
			N	58	1.2	−0.7	3.6	88.7	146.6	2.6					
			R	10	181.9	0.6	8								
Loiyangalani	2.6	36.5	C	32	1.1		4.1	86.5	197.6	2.9	31.6	77	$9.8^{11.7}_{7.9}$	$9.3^{11.1}_{7.9}$	14
			N	15	358.6	−1.1	4.7	85.9	219.1	3					
			R	17	183.4	0.8	6.7	88.3	207.1	5.2					
Costa Rica	10	276	C	28	2.1	14.2	8.2	86.8	58.2	5.9	26.8	22	$17.6^{22.2}_{13.1}$	$17.2^{21.0}_{14.9}$	15
			N	24	0.9	16.8	8.5	88.7	60.8	6					
Afar, Ethiopia	12	41.5	C	103	2.9	14.8	3.1	85.3	186.4	2.2	100.5	41.5	$13.4^{14.8}_{11.9}$	$12.6^{13.9}_{11.5}$	16
			N	53	3.0	19.9	3.2	86.9	154.5	2.6					
			R	50	182.9	−9.2	5	−82.9	20.7	3.5					
Guadalupe Island	16	298	N	25	0.5	30.2	4.1	89.3	348	3.7	63	26.9		$10.2^{12.6}_{8.6}$	17

Table 3. (continued)

Location	Latitude (deg)	Longitude (deg)	P	N	Dec	Inc	α_{95}	Pal.Pole Latitude	Pal.Pole Longitude	A_{95}	R	K	Sb1 "T"	Sb2 "C"	References[b]
Mexico	19.6	261	C	185	359	32	2	88	123.6	1.6	180.7	42.6	$12.5^{13.}_{11.4}$	$12.4^{13.4}_{11.6}$	18
			N	135	359	30.2	2.2	87.3	107.6	1.8					
			R	50	178.2	−34.5	3.6	−88	11.8	3.2					
Hawaii	21.3	202	C	118	1.4	28.1	2.2	84.1	5.7	1.8	115.8	53.5	$12.5^{13.9}_{11.4}$	$11.1^{12.2}_{10.2}$	19
			N	108	1.8	27.8	2.3	83.7	1.9	1.9					
			R	10	176.5	−30.7	9.3								
La Palma Island	28.8	342	C	21	358	41.4	6.1	85.2	189.3	7	16.4	26.9		$15.6^{20.3}_{12.7}$	20
			N	9	355.1	46.1	9.6	81.6	251.4	13.8					
			R	12	180.9	−39.1	8.4	84	337.9	8.6					
Southwest	35.4	248.2	C	54	355.7	53.8	3.1	86.1	150.6	3.5	52.3	30.8	$15.0^{17.2}_{12.7}$	$14.6^{16.8}_{12.9}$	21
			N	35	354	54.9	4.4	84.5	167.9	4.8					
			R	19	178.6	−51.7	4	−86.7	267.5	4.9					
Sao Miguel	37	335	C	27	357.4	48.2	5.4	82.3	171	5.6	26	25.6	$17.9^{22.3}_{13.8}$	$16^{17.4}_{13.5}$	22
			N	14	359.2	52.1	7.9	86.5	167.7	7.8					
			R	13	175.7	−43.9	7.6	77.7	172	8.2					
Northern California and Idaho	39–43.5	247	C	33	3.5	58.3	4.1	87.9	231.9	5.1	31.7	24.6	$16.4^{18.4}_{14.2}$	$16.3^{19.6}_{14}$	23
			N	15	7	59.4	6.7	87.3	230.7	8.3					
			R	18	180.8	−57.3	5.4	−88.3	53.4	7					
Washington	46	238.3	N	56	2.6	65.2	2.5	87.3	270	3.6	54.1	28.7	$15.3^{18.4}_{14}$	$15.1^{17.1}_{13.4}$	24
British Columbia	51	240	N	49	356.9	69.9	2.8	86	214.3	4.2	47	24.3	$16.8^{19.5}_{14}$	$16.4^{19}_{14.4}$	25
Aleutions	53	192	C	75	358.6	70.7	2.6	86.3	184.1	4.3	70.3	15.7	$21^{25.4}_{16.5}$	$20.4^{22.9}_{19}$	26
			N	62	356.8	68.1	2	89.3	88.2	3					
			R	13	207	−82.9	18.1	62.8	205.9	18.1					
Nunivak	60	194	C	50	2.8	75	2.8	87	214.2	4.6	47.6	20	$18.3^{20.8}_{15.6}$	$18.1^{21}_{15.9}$	27
			N	36	359.8	74.6	2.8	88.1	193	4.7					
			R	14	191.5	−75.9	7.3	83.4	50.5	12.1					
Iceland	65.1	345	C	38	0.4	74.3	4.2	87.5	148.1	7	34.9	11.9	$23.7^{27.7}_{20}$	$23.5^{27.9}_{20.3}$	28
			N	13	358.9	77.2	8.9	86.9	339	14.6					
			R	25	180.9	−72.8	4.8	84.7	151.2	8					

[a]Pal.Pole means paleomagnetic pole. Sb1 "T" are the errors following the bootstrap method of *Tauxe* [2009], while Sb2 "C" are the errors according to *Cox* [1969].

[b]References are as follows: 1, *Lawrence et al.* [2009]; 2, *Baraldo et al.* [2003]; 3, *Mejia et al.* [2004]; 4, *Camps et al.* [2001]; 5, *Tanaka et al.* [1996, 1997, 2008]; 6, *Opdyke and Musgrave* [2004]; 7, *Quidelleur et al.* [2009]; 8, *Brown* [2002] and *Miki et al.* [1998]; 9, L. Brown cited by *Johnson et al.* [2008]; 10, *Yamamoto et al.* [2002]; 11, *Elmaleh et al.* [2004]; 12, *Opdyke et al.* [2006]; 13, Mount Kenya (this paper); 14, Loiyangalani (this paper); 15, C. Constable et al. cited by *Johnson et al.* [2008]; 16, *Kidane et al.* [2003]; 17, *Carlut et al.* [2000]; 18, *Mejia et al.* [2005]; 19, *Laj et al.* [1999] and *Herrero-Bervera and Valet* [2002, 2003, 2007]; 20, *Tauxe et al.* [2000]; 21, *Tauxe et al.* [2003]; *Mankinen* [2008]; 22, *Johnson et al.* [1998]; 23, *Tauxe et al.* [2004]; *Mankinen* [2008]; 24, *Mitchell et al.* [1989]; 25, *Mejia et al.* [2002]; 26, *Stone and Layer* [2006]; 27, R. Coe cited by *Johnson et al.* [2008]; 28, *Udagawa et al.* [1999].

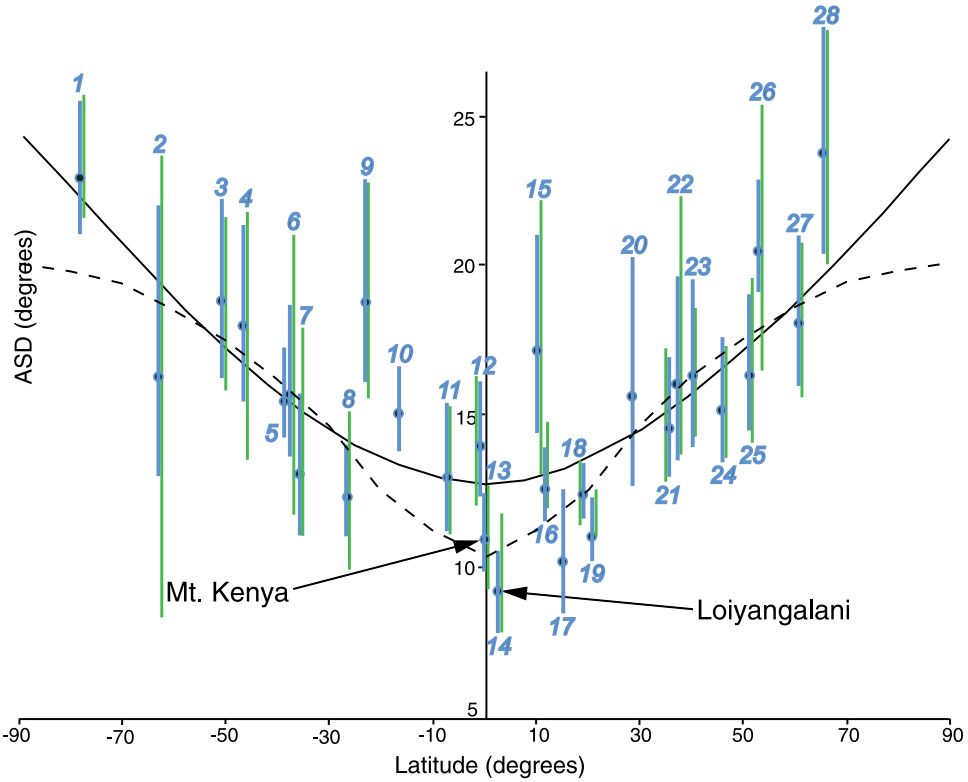

Figure 12. The dispersion (Sb) plotted against latitude for modern studies that meet the selection criteria used in this study. The plotted error limits Sb are calculated by *Cox*'s [1969] method (blue) and using the bootstrap method (green) of *Tauxe* [2009]. Data are presented in Table 3. Shown for comparison is TK03 model of *Tauxe and Kent* [2004] (dashed line) and original Model G of *McFadden et al.* [1988] (solid line).

equator. *Tauxe and Kent* [2004] have provided another model (TK03) that was tuned to updated Model G of *McElhinny and McFadden* [1997] and thus also agrees with the Kenya results (Figure 12). The modern variation of inclination along the equator ranges from +20° in South America to −20° in Africa. The data presented have inclination values that exceed this and we have eleven inclination values that are greater than 20° with one as high as 35.6°.

[29] The VGP dispersion (Figure 12) at Loiyangalani is low (Sb = 9.5°, 95% confidence interval from 7.4° to 11.3°), in agreement with what we observe at Mount Kenya (10.9°) and less than the dispersion that we measured in Ecuador. There can be little doubt the VGP dispersion is low at the equator and about the value estimated in updated Model G of *McElhinny and McFadden* [1997] or by *Tauxe and Kent* [2004]. These observations are not in agreement with a recent paper by *Johnson et al.* [2008]. The data reported by them are interpreted as being invariant with latitude, which is not in agreement with the data presented here. The decrease in dispersion with latitude appears to be steady from high to low latitude when determined from high-quality studies which have sufficient samples per site, and that have been demagnetized using modern techniques. For example, the recent publication of an excellent large data set from Antarctica (N = 112 [*Lawrence et al.*, 2009]) yields an Sb of 23.7°, which is 12° higher than we observe at Mount Kenya and well outside the error limits; likewise, data from Iceland have an Sb value of 23.7° (Table 3). The increase of dispersion from low to high latitude is supported by a recent study by *Harrison* [2009] who used a different data set from than used in this paper.

[30] The database presented in Table 3 will undoubtedly improve with time as more and larger studies are added. Some of the data are from studies that are too small with acceptable sites numbering less than 20, whereas more recent studies have tended to have larger numbers of sites numbering 50 or more. It is interesting that several studies from the high Andes (Atacama, Ecuador) have higher dispersion than adjacent localities. The data from Hawaii no longer seems to have unusually low dispersion.

Acknowledgments

[31] We wish to express our thanks to the National Science Foundation for funding this study in Kenya with grants to the University of Florida (NSF EAR0608998) and Rutgers University (EAR0609339). We thank Lisa Tauxe for help in the application of the bootstrap method of determining the errors on Sb. We would like to thank the Department of Physics at the University of Nairobi for logistical support. We would like to thank the Government of Kenya who issued us permits to collect samples and to ship them to the United States. We are grateful to Concorde Car Hire who provided the drivers and vehicles that allowed us to survive in occasionally difficult field conditions. This paper is LDEO contribution 7329.

References

Baker, B. H. (1967), Geology of the Mount Kenya area, *Rep. 79*, 78 pp., Geol. Surv. of Kenya, Nairobi.

Baker, B. H., L. A. Williams, J. A. Miller, and F. J. Fitch (1971), Sequence and geochronology of the Kenya Rift volcanics, *Tectonophysics*, *11*, 191–215, doi:10.1016/0040-1951(71)90030-8.

Baraldo, A., A. E. Rapalini, H. Boehnel, and M. Mena (2003), Paleomagnetic study of Deception Island, South Shetland Islands, Antarctica, *Geophys. J. Int.*, *153*, 333–343, doi:10.1046/j.1365-246X.2003.01881.x.

Biggin, A. J., H. M. Geert, M. A. Strik, and C. G. Langereis (2008), Evidence for a very long term trend in geomagnetic secular variation, *Nat. Geosci.*, *1*, 395–398, doi:10.1038/ngeo181.

Brotzu, P., L. Morbidelli, M. Nicoletti, E. M. Piccirillo, and G. Traversa (1984), Miocene to Quaternary volcanism in eastern Kenya: Sequence and geochronology, *Tectonophysics*, *101*, 75–86, doi:10.1016/0040-1951(84)90043-X.

Brown, L. (2002), Paleosecular variation from Easter Island revisited: Modern demagnetization of a 1970's data set, *Phys. Earth Planet. Inter.*, *133*, 73–81.

Camps, P., B. Henry, M. Prevot, and L. Faynot (2001), Geomagnetic secular variation recorded in Plio-Pleistocene volcanic rocks from Possession Island (Crozet Archipelago southern Indian Ocean), *J. Geophys. Res.*, *106*, 1961–1971, doi:10.1029/2000JB900370.

Carlut, J., X. Quidelleur, V. Courtillot, and G. Boudon (2000), Paleomagnetic directions and K/Ar dating of 0 to 1 Ma lava flows from La Guadalupe Island (French West Indies): Implications for time-averaged field models, *J. Geophys. Res.*, *105*, 835–849, doi:10.1029/1999JB900238.

Class, C., R. Altherr, F. Volker, G. Eberz, and M. T. McCulloch (1994), Geochemistry of Pliocene to Quaternary alkali basalts from the Hurri Hills, northern Kenya. 1994, *Chem. Geol.*, *113*, 1–22, doi:10.1016/0009-2541(94)90002-7.

Cox, A. (1969), Confidence limits for the precision parameter k, *Geophys. J. R. Astron. Soc.*, *18*, 545–549.

Cox, A. (1971), Paleomagnetism of San Cristobal Island, Galapagos, *Earth Planet. Sci. Lett.*, *11*, 152–160, doi:10.1016/0012-821X(71)90158-0.

Day, R., M. D. Fuller, and V. A. Schmidt (1977), Hysteresis properties of titanomagnetites: Grain size and composition dependence, *Phys. Earth Planet. Inter.*, *13*, 260–267, doi:10.1016/0031-9201(77)90108-X.

Elmaleh, A., J. -P. Valet, X. Quidelleur, A. Solihin, H. Bouquerel, T. Tesson, E. Mulyadi, A. Khokhlov, and A. D. Wirakusumah (2004), Paleosecular variation in Java and Bawean Islands (Indonesia) during the Brunhes Chron, *Geophys. J. Int.*, *157*, 441–454, doi:10.1111/j.1365-246X.2004.02197.x.

Fisher, R. A. (1953), Dispersion on a sphere, *Proc. R. Soc. London, Ser. A*, *217*, 295–305, doi:10.1098/rspa.1953.0064.

Foster, D. A., and A. J. W. Gleadow (1996), Structural framework and denudation history of the flanks of the Kenya and Anza rifts, East Africa, *Tectonics*, *15*, 258–271, doi:10.1029/95TC02744.

Foster, D. A., B. D. Goscombe, and D. R. Gray (2009), Rapid exhumation of deep crust in an convergent orogen: The Kaoko Belt of the Damara Orogen, *Tectonics*, *28*, TC4002, doi:10.1029/2008TC002317.

Gathogo, P. N., F. H. Brown, and I. McDougall (2008), Stratigraphy of the Koobi Formation (Pliocene and Pleistocene) in the Loiyangolani region of northern Kenya, *J. Afr. Earth Sci.*, *51*, 277–297, doi:10.1016/j.jafrearsci.2008.01.010.

Harrison, C. G. A. (2009), Latitudinal signature of Earth's magnetic field variation over the last 5 million years, *Geochem. Geophys. Geosyst.*, *10*, Q02012, doi:10.1029/2008GC002298.

Herrero-Bervera, E., and J. P. Valet (2002), Paleomagnetic secular variation of the Honolulu volcanic Series (33–700 ka), O'ahu (Hawaii), *Phys. Earth Planet. Inter.*, *133*, 83–97, doi:10.1016/S0031-9201(02)00092-4.

Herrero-Bervera, E., and J. P. Valet (2003), Persistent anomalous inclinations recorded in the Koolau volcanic series on the island of Oahu (Hawaii, USA) between 1.8 and 2.6 Ma, *Earth Planet. Sci. Lett.*, *212*, 443–456, doi:10.1016/S0012-821X(03)00168-7.

Herrero-Bervera, E., and J. P. Valet (2007), Holocene paleosecular variation from dated lava flows on Maui (Hawaii), *Phys. Earth Planet. Inter.*, *161*, 267–280, doi:10.1016/j.pepi.2007.02.008.

Johnson, C. L., et al. (2008), Recent investigations of the 0–5 Ma geomagnetic field recorded by lava flows, *Geochem. Geophys. Geosyst.*, *9*, Q04032, doi:10.1029/2007GC001696.

Johnson, H. L., J. R. Wijbrans, C. G. Constable, J. Gee, H. Staudigall, L. Tauxe, V. H. Forjaz, and M. Salgiero (1998), Ar/Ar ages and paleomagnetism of Sao Migel lavas, *Azores*, *Earth Planet. Sci. Lett.*, *160*, 637–649, doi:10.1016/S0012-821X(98)00117-4.

Kidane, T., V. Courtillot, I. Manighetti, L. Audin, P. Lahitte, X. Quidelleur, P. -Y. Gillot, Y. Gallet, J. Carlut, and T. Haile (2003), New paleomagnetic and geochronologic results from Ethiopian Afar: Block rotations linked to rift overlap and propagation and determination of a –2 Ma reference pole for stable Africa, *J. Geophys. Res.*, *108*(B2), 2102, doi:10.1029/2001JB000645.

Kirschvink, J. L. (1980), The least squares line and plane and the analysis of paleomagnetic data, *Geophys. J. R. Astron. Soc.*, *62*, 699–718.

Koppers, A. A. P. (2002), ArAr CALC software for $^{40}Ar/^{39}Ar$ age calculations, *Comput. Geosci.*, *28*, 605–619, doi:10.1016/S0098-3004(01)00095-4.

Laj, C., H. Guillou, N. Szeremeta, and R. Coe (1999), Geomagnetic secular variation at Hawaii around 3 Ma from a sequence of 107 lava flows from Kaena Point (Oahu), *Earth Planet. Sci. Lett.*, *170*, 365–376, doi:10.1016/S0012-821X(99)00119-3.

Lawrence, K. P., L. Tauxe, H. Staudigal, C. G. Constable, A. Koppens, W. McIntosh, and C. L. Johnson (2009), Paleomagnetic field properties at high southern latitude,

Geochem. Geophys. Geosyst., *10*, Q01005, doi:10.1029/2008GC002072.

Mankinen, E. A. (2008), Paleomagnetic study of late Miocene through Pleistocene igneous rocks from the southwestern USA: Results from the historic collections of the U. S. Geological Survey Menlo Park laboratory, *Geochem. Geophys. Geosyst.*, *9*, Q05017, doi:10.1029/2008GC001957.

McElhinny, M. W., and P. L. McFadden (1997), Paleosecular variation over the past 5 Myr based on a new generalized database, *Geophys. J. Int.*, *131*, 240–252, doi:10.1111/j.1365-246X.1997.tb01219.x.

McFadden, P. L., R. T. Merrill, and M. W. McElhinny (1988), Dipole/quadrupole family modeling of paleosecular variation, *J. Geophys. Res.*, *93*, 11,583–11,588, doi:10.1029/JB093iB10p11583.

Mejia, V., R. W. Barendregt, and N. D. Opdyke (2002), Paleosecular variation of brunhes age lava flows from British Columbia, Canada, *Geochem. Geophys. Geosyst.*, *3*(12), 8801, doi:10.1029/2002GC000353.

Mejia, V., N. D. Opdyke, J. Vilas, B. S. Singer, and J. S. Stoner (2004), Paleomagnetic secular variation of Pliocene-Quaternary lava flows from southern Patagonia, *Geochem. Geophys. Geosyst.*, *5*, Q03H08, doi:10.1029/2003GC000633.

Mejia, V., H. Bohnel and N. D. Opdyke (2005), Paleosecular variation and time-averaged field recorded in late Pliocene–Holocene lava flows from Mexico, *Geochem. Geophys. Geosyst.*, *6*, Q07H19, doi:10.1029/2004GC000871.

Miki, M., H. Inokuchi, S. Yamaguchi, J. Matsuda, K. Nagao, N. Isazaki, and K. Yaskawa (1998), Geomagnetic secular variation in Easter Island, southeast Pacific, *Phys. Earth Planet. Inter.*, *106*, 93–101, doi:10.1016/S0031-9201(97)00106-4.

Mitchell, R. J., D. J. Jaeger, J. F. Diehl, and P. E. Hammond (1989), Paleomagntic results from the Indian Heaven volcanic field, south central Washington, *Geophys. J. R. Astron. Soc.*, *97*, 381–390.

Ochieng, J. O., A. F. Wilkinson, J. Kagasi, and S. Kimomo (1988), The geology of the Loiyangalani area, *Rep. 107*, 53 pp., Mines and Geol. Dep., Min. of Environ. and Nat. Resour., Nairobi.

Opdyke, N. D., and V. Mejia (2004), Earth's magnetic field, in *Timescales of the Paleomagnetic Field*, *Geophys. Monogr. Ser.*, vol. 145, edited by J. Channell et al., pp. 315–320, AGU, Washington, D. C.

Opdyke, N. D., and R. Musgrave (2004), Paleomagnetic results from the Newer Volcanics of Victoria: Contribution to the Time Averaged Field Initiative, *Geochem. Geophys. Geosyst.*, *5*, Q03H09, doi:10.1029/2003GC000632.

Opdyke, N. D., M. Hall, V. Mejia, K. Huang, and D. A. Foster (2006), Time-averaged field at the equator: Results from Ecuador, *Geochem. Geophys. Geosyst.*, *7*, Q11005, doi:10.1029/2005GC001221.

Quidelleur, X., J. Carlut, P. Tchilinguirian, A. Germa, and P.-Y. Gillot (2009), Paleomagnetic study from mid-latitude sites in the southern hemisphere (Argentina): Contribution to time averaged field modals, *Phys. Earth Planet. Inter.*, *172*, 199–209, doi:10.1016/j.pepi.2008.09.012.

Reilly, T. A., P. K. S. Raja, A. E. Mussett, and A. Brock (1976), The palaeomagnetism of Late Cenozoic volcanic rocks from Kenya and Tanzania, *Geophys. J. R. Astron. Soc.*, *45*, 483–494.

Renne, P. R., C. C. Swisher, A. I. Deino, D. B. Karner, T. I. Owens, and D. J. DePaulo (1998), Intercalibration of standards, absolute ages and uncertainties in $^{40}Ar/^{39}Ar$ dating, *Chem. Geol.*, *145*, 117–152, doi:10.1016/S0009-2541(97)00159-9.

Rix, P. (1967), Geology of the Kinna area, *Rep. 84*, Geol. Surv. of Kenya, Nairobi.

Schneider, D. A., and D. V. Kent (1988), The paleomagnetic field from equatorial deep-sea sediments: Axial symmetry and polarity asymmetry, *Science*, *242*, 252–256, doi:10.1126/science.242.4876.252.

Smirnov, A. V., and J. A. Tarduno (2004), Secular variation of the Late Archean–Early Proterozoic geodynamo, *Geophys. Res. Lett.*, *31*, L16607, doi:10.1029/2004GL020333.

Stone, D. B., and P. W. Layer (2006), Paleosecular variation and GAD studies of 0–2 Ma flow sequences from the Aleutian Islands, Alaska, *Geochem. Geophys. Geosyst.*, *7*, Q04H22, doi:10.1029/2005GC001007.

Tanaka, H., G. M. Turner, B. F. Houghton, T. Tchibana, M. Kono, and M. O. McWilliams (1996), Paleomagnetism and chronology of the Central Taupo Volcanic Zone, New Zealand, *Geophys. J. Int.*, *124*, 919–934, doi:10.1111/j.1365-246X.1996.tb05645.x.

Tanaka, H., K. Kanamura, K. Nagao, and B. F. Houghton (1997), K-Ar Ages and paleosecular variation of direction and intensity from Quaternary lava sequences in the Ruapehu Volcano, New Zealand, *J. Geomagn. Geoelectr.*, *49*, 587–599.

Tanaka, H., N. Komuro, and G. M. Turner (2008), Paleosecular variation for 0.1–21 Ka from the Okataina Volcanic Center, New Zealand, *Earth Planets Space*, *60*, 1–13.

Tauxe, L. (2009), *Essentials of Paleomagnetism*, 485 pp., Univ. of Calif. Press, Berkley.

Tauxe, L., and D. V. Kent (2004), A simplified statistical model for the geomagnetic field and the detection of shallow bias in paleomagnetic inclinations: Was the ancient magnetic field dipolar?, in *Timescales of the Paleomagnetic Field*, *Geophys. Monogr. Ser.*, vol. 145, edited by J. E. T. Channell et al., pp. 101–115, AGU, Washington, D. C.

Tauxe, L., H. Staudigel, and J. R. Wijbrans (2000), Paleomagnetism and $^{40}Ar/^{39}Ar$ ages from La Palma in the Canary Islands, *Geochem. Geophys. Geosyst.*, *1*(9), 1038, doi:10.1029/2000GC000063.

Tauxe, L., C. G. Constable, C. Johnson, A. A. P. Koppers, W. R. Miller, and H. Staudigel (2003), Paleomagnetism of the southwestern U.S.A. recorded by 0–5 Ma igneous rocks, *Geochem. Geophys. Geosyst.*, *4*(4), 8802, doi:10.1029/2002GC000343.

Tauxe, L., P. Selkin, A. Gans, and A. Calvert (2004), Paleomagnetic results from the Snake River Plain: Contribution to the time-averaged field global database, *Geochem. Geophys. Geosyst.*, *5*, Q08H13, doi:10.1029/2003GC000661.

Udagawa, S., H. Kitagawa, A. Gudmunson, O. Hiroi, T. Koyagutchi, H. Tanaka, I. Kirstjansonn, and M. Kono (1999), Age and magnetism in the Jokuldalur area, eastern Iceland: Gilsá event revisited, *Phys. Earth Planet. Inter.*, *115*, 147–171, doi:10.1016/S0031-9201(99)00073-4.

Wilson, R. L. (1970), Permanent aspects of the Earth's non-dipole magnetic field over Upper Tertiary times, *Geophys. J. R. Aston. Soc.*, *19*, 417–437.

Wilson, R. L. (1972), Palaeomagnetic differences between normal and reversed field sources, and the problem of far-sided and right-handed pole positions, *Geophys. J. R. Aston. Soc.*, *28*, 295–304.

Yamamoto, Y., K. Shimura, H. Tsunakawa, T. Kogiso, K. Uto, H. G. Barsczus, H. Oda, T. Yamazaki, and E. Kikawa, (2002), Geomagnetic paleosecular variation for the past 5 Ma in the Society Islands, French Polynesia, *Earth Planets Space*, *54*, 797–80.